mathematics

MDPI

Article

On Chaos and Complexity Analysis for a New Sine-Based Memristor Map with Commensurate and Incommensurate Fractional Orders

Tareq Hamadneh [1], Abderrahmane Abbes [2,*], Hassan Al-Tarawneh [3], Gharib Mousa Gharib [4], Wael Mahmoud Mohammad Salameh [5], Maha S. Al Soudi [6] and Adel Ouannas [7]

[1] Department of Mathematics, Faculty of Science, Al Zaytoonah University of Jordan, Amman 11931, Jordan; t.hamadneh@zuj.edu.jo
[2] Laboratory of Mathematics, Dynamics and Modelization, Badji Mokhtar-Annaba University, Annaba 23000, Algeria
[3] Department of Data Sciences and Artificial Intelligence, Al-Ahliyya Amman University, Amman 11931, Jordan; h.altarawneh@ammanu.edu.jo
[4] Department of Mathematics, Faculty of Science, Zarqa University, Zarqa 13110, Jordan; ggharib@zu.edu.jo
[5] Faculty of Information Technology, Abu Dhabi University, Abu Dhabi 59911, United Arab Emirates; wael.salameh@adu.ac.ae
[6] Department of Basic Scientific Sciences, Applied Science Private University, Amman 11931, Jordan; m_alsoudi@asu.edu.jo
[7] Department of Mathematics and Computer Science, University of Larbi Ben M'hidi, Oum El Bouaghi 04000, Algeria; ouannas.adel@univ-oeb.dz
* Correspondence: abderrahmane.abbes@univ-annaba.dz

Abstract: In this study, we expand a 2D sine map via adding the discrete memristor to introduce a new 3D fractional-order sine-based memristor map. Under commensurate and incommensurate orders, we conduct an extensive exploration and analysis of its nonlinear dynamic behaviors, employing diverse numerical techniques, such as analyzing Lyapunov exponents, visualizing phase portraits, and plotting bifurcation diagrams. The results emphasize the sine-based memristor map's sensitivity to fractional-order parameters, resulting in the emergence of distinct and diverse dynamic patterns. In addition, we employ the sample entropy ($SampEn$) method and C_0 complexity to quantitatively measure complexity, and we also utilize the 0–1 test to validate the presence of chaos in the proposed fractional-order sine-based memristor map. Finally, MATLAB simulations are be executed to confirm the results provided.

Keywords: chaos; sine memristor map; discrete fractional calculus; complexity

MSC: 37M20

Citation: Hamadneh, T.; Abbes, A.; Al-Tarawneh, H.; Gharib, G.M.; Salameh, W.M.M.; Al Soudi, M.S.; Ouannas, A. On Chaos and Complexity Analysis for a New Sine-Based Memristor Map with Commensurate and Incommensurate Fractional Orders. *Mathematics* **2023**, *11*, 4308. https://doi.org/10.3390/math11204308

Academic Editors: Chunhua Wang and Hairong Lin

Received: 31 August 2023
Revised: 30 September 2023
Accepted: 6 October 2023
Published: 16 October 2023

1. Introduction

A memory resistor, commonly known as a "memristor", has been widely recognized as a fourth fundamental circuit element that serves as a link between charge and magnetic flux. The theoretical concept of the memristor was initially forwarded by Chua in 1971 [1]. For an extended period, Memristor research remained primarily theoretical until the first physical implementation of a memristor was achieved by HP laboratories in 2008. They successfully developed the first practical memristor using nanomaterials [2]. It has since become an essential component in various applications due to its unique properties and potential to revolutionize memory and computing technologies. Memristors have garnered significant attention and research interest, contributing to advancements in various fields, including electronics [3], computing [4], nonvolatile memory [5], and neuromorphic systems [6].

Chaos theory (Devaney 1989) is the concept that a slight now might lead to a significant change later. It is a mathematical branch with applications in physics, economics, engineer-

ing, and biology [7–14]. The presence of randomness and unpredictability in chaotic systems and the sensitivity to initial conditions allow for the generation of pseudo-random sequences and enhanced data encryption. These inherent merits of chaotic behaviors have contributed to significant progress in various fields, including secure communications, image and signal processing, data encryption, and optimization algorithms, among others [15–18]. The rich dynamics of chaotic systems continue to inspire novel research and applications, making chaos theory an essential area of study with broad interdisciplinary impact.

Fractional chaotic behaviors are extensively seen in both social and natural sciences, attracting considerable interest from various domains. In recent years, discrete-time fractional calculus has attracted much interest due to its significance in real-world challenges [19–26]. These studies have reflected that the system's behavior is highly dependent on the chosen fractional order, showcasing its non-linear and complex nature, which makes it a fascinating subject of study in the field of fractional dynamics.

In general, discrete-time memristive maps have not been extensively discussed compared to the continuous-time domain. In practice, discrete chaotic systems offer the advantage of avoiding parameter sensitivity issues present in continuous systems, making them easier to implement using digital hardware circuits [27]. Consequently, the study of discrete fractional memristors remains inadequate, with relatively few studies dedicated to exploring their behavior and characteristics. For example, the investigation of the chaotic behaviors in the Caputo fractional memristive map has been studied in [28]. The development of a 2D discrete memristor map by incorporating a memristor into a 1D Rulkov neuron map has been presented in [29]. The multistability and synchronization of fractional maps resulting from the coupling of Rulkov neurons with locally active discrete memristors have been conducted by Ma et al. in [30]. The hidden attractors and multistability in a fractional non-fixed-point discrete-memristor-based map have been investigated by Shatnawi et al. [31]. Peng et al. [32] have studied the fractional-memristor-based discrete chaotic map using the Grunwald–Letnikov operator. Furthermore, Khennaoui et al. [33] developed the Lozi map to introduce the fractional memristor Lozi map and discussed their hidden chaotic dynamics. Most of these studies have predominantly focused on commensurate-order models in discrete-memristor-based maps. However, there appears to be a noticeable gap in the literature concerning the effect of the incommensurate-order case on the dynamics of such maps. This indicates an underexplored area in the field of discrete memristors, particularly in the context of incommensurate fractional memristors. Understanding the behavior and properties of incommensurate fractional memristors could lead to valuable insights and potential applications in various domains. Therefore, further investigation and research in this area are essential to uncovering the unique characteristics and potential benefits of incommensurate fractional memristors.

Inspired by the preceding discussion, our objectives in this work are summarized as follows:

1. A new 3D fractional-order sine-based memristor map is presented by establishing a connection between the 2D sine map and the discrete memristor.
2. The dynamical properties are comprehensively explored, and some basic dynamical characteristics demonstrated by this map, such as phase portraits, bifurcation diagrams, and the maximum Lyapunov exponent, are investigated using a range of fractional values, encompassing both commensurate and incommensurate cases.
3. To quantitatively measure complexity and validate the presence of chaos within the proposed sine-based memristor map, we give the C_0 complexity, sample entropy test ($SampEn$), and 0–1 test results.

The rest of this manuscript is structured as follows: In Section 2, we give some essential preliminary concepts of fractional discrete calculus. In Section 3, we introduce the mathematical model of the 3D fractional sine-based memristor map. In Section 4, we delve into an analysis of the dynamic characteristics of the fractional sine-based memristor map, focusing on both commensurate and incommensurate scenarios. This exploration is facilitated through Lyapunov exponent analysis, bifurcation diagrams, and phase attractor

visualization. In Section 5, we use the C_0 complexity, sample entropy test, ($SampEn$), and 0–1 test to quantitatively measure complexity and validate the presence of chaos within the map. Finally, we conclude the paper by summarizing the most noteworthy findings obtained throughout the study.

2. Preliminaries

To elucidate our memristor framework, we first provide a specific overview within the domain of discrete fractional calculus.

Definition 1 ([34]). *The β-th fractional sum for a function Y can be expressed as:*

$$\Delta_b^{-\beta} Y(v) = \frac{1}{\Gamma(\beta)} \sum_{l=b}^{b-\beta} (b-1-l)^{(\beta-1)} Y(l), \tag{1}$$

where $v \in \mathbb{N}_{b+\beta}$, $\beta > 0$ and $\mathbb{N}_b = \{b, b+1, b+2, \cdots\}$.

Definition 2 ([35]). *The Caputo-like difference operator for a function $Y(v)$ can be stated as:*

$${}^{C}\Delta_v^{\beta} Y(b) = \Delta_b^{-(m-\beta)} \Delta^m X(v) = \tfrac{1}{\Gamma(m-\beta)} \textstyle\sum_{l=b}^{v-(m-\beta)} (v-l-1)^{(m-\beta-1)} \Delta^m Y(l), \tag{2}$$

where $v \in \mathbb{N}_{b+m-\beta}$, $\beta \notin \mathbb{N}$ and $m = \lceil \beta \rceil + 1$. $\Delta^m Y(v)$ and $(v-l-1)^{(m-\beta-1)}$ are the m-th integer difference operator and the falling factorial function, respectively, which are written as

$$\Delta^m Y(v) = \Delta(\Delta^{m-1} Y(v)) = \sum_{k=0}^{m} \binom{m}{k} (-1)^{m-k} Y(v+k), \qquad v \in \mathbb{N}_b, \tag{3}$$

and

$$(v-1-l)^{(m-\beta-1)} = \frac{\Gamma(v-l)}{\Gamma(v+1-l-m+\beta)}, \tag{4}$$

Remark 1. *For $m = 1$, we can define the Caputo-like operator by*

$${}^{C}\Delta_b^{\beta} Y(v) = \Delta_b^{-(1-\beta)} \Delta Y(v) = \tfrac{1}{\beta(1-\beta)} \textstyle\sum_{l=b}^{v-(1-\beta)} (v-1-l)^{(-\beta)} \Delta Y(l), \quad v \in \mathbb{N}_{b-\beta+1} \tag{5}$$

Theorem 1 ([19]). *The solution to the following fractional difference system*

$$\begin{cases} {}^{C}\Delta_b^{\beta} Z(v) = Y(v+\beta-1, Z(v+\beta-1)) \\ \Delta^j Z(v) = Z_j, \quad m = \lceil \beta \rceil + 1, \end{cases} \tag{6}$$

is expressed by

$$Z(v) = Z_0(v) + \frac{1}{\Gamma(\beta)} \sum_{l=m-\beta}^{v-\beta} (v+1-l)^{(\beta-1)} Y(l-1+\beta, Z(l-1+\beta)), \quad v \in \mathbb{N}_{b+m}, \tag{7}$$

where

$$Z_0(v) = \sum_{j=0}^{m-1} \frac{(v-b)^j}{\Gamma(j+1)} \Delta^j Z(0). \tag{8}$$

3. Fractional-Order Sine-Based Memristor Map

The original work of Bao et al. [36] introduced the 2D sine map, which is written as:

$$\begin{cases} y_1(r+1) = y_1(r) + \alpha_1 \sin(y_2(r)), \\ y_2(r+1) = y_2(r) + \alpha_2 \sin(y_1(r)) \sin(y_2(r)), \end{cases} \tag{9}$$

where α_1 and α_2 are adjustable parameters.

A memristor is a two-terminal nonlinear device that displays a pinched hysteresis in response to the application of any periodic voltage or current stimulation. Diverse memristors with discrete memristance values have been suggested through the use of differential modeling theory [37]. As per the concept presented in reference [38], the discrete memristor can be defined by:

$$\begin{cases} v_r = M(q_r) i_r, \\ q_{r+1} = q_r + k\, i_r, \end{cases} \tag{10}$$

where v_r represents the output voltage, i_r is the input current, and q_r represents the internal state of the discrete memristor at step r. $M(q_r)$ denotes the value of the discrete memristance function, which is equal, in this study, to

$$M(q_r) = \sin q_r.$$

Thus, the mathematical model for the discrete memristor (10) is formulated by

$$\begin{cases} v_r = \sin(q_r) i_r, \\ q_{r+1} = q_r + k\, i_r. \end{cases} \tag{11}$$

To expand the dimension of the proposed sine map, we incorporate the discrete memristor model (11) into the map (9) by adding the voltage v_r of the memristor to the y_1 variable. Furthermore, the variables y_2 and y_3 correspond to the current i_r and the internal state r_r of Equation (11). Thus, the dimension of the sine map is increased, yielding the following 3D sine-based memristor map:

$$\begin{cases} y_1(r+1) = y_1(r) + \alpha_1 \sin\left((y_2(r)) + \mu y_2(r) \sin(y_3(r))\right), \\ y_2(r+1) = y_2(r) + \alpha_2 \sin(y_1(r)) \sin(y_2(r)), \\ y_3(r+1) = y_3(r) + k y_2(r), \end{cases} \tag{12}$$

where μ is the controller parameter and k is the step size. Figure 1 illustrates a bifurcation diagram and Lyapunov exponent, as well as the phase attractor of the 3D sine-based memristor map while varying α_2 from 1 to 4. The initial conditions are chosen as $y_1(0) = -2$ $y_2(0) = 1$, and $y_3(0) = 0.1$, and the parameters are chosen as $\alpha_1 = 1.5$, $\mu = 0.1$, and $k = 0.01$. The evidence presented in Figure 1 provides that the model demonstrates chaotic dynamics for a significant range of values of α_1 and α_2, specifically within the interval $\alpha_2 \in (3.23, 4)$.

In this investigation, we extend the integer-order sine-based memristor map to generate the fractional-order sine-based memristor map by employing the Caputo difference operator. The formula representing the first-order difference in the sine-based memristor map is as follows:

$$\begin{cases} \Delta y_1(r) = \alpha_1 \sin\left((y_2(r)) + \mu y_2(r) \sin(y_3(r))\right), \\ \Delta y_2(r) = \alpha_2 \sin(y_1(r)) \sin(y_2(r)), \\ \Delta y_3(r) = k y_2(r), \end{cases} \tag{13}$$

where $\Delta y(r) = y(r+1) - y(r)$ is the standard difference operator. In the aforementioned system, if we substitute Δ with the Caputo-like operator ${}^{c}\Delta_b^{\beta}$ and replace r with $\varrho = v + \beta - 1$, the resulting system becomes a fractional-order difference system.

$$\begin{cases} {}^{c}\Delta_b^{\beta} y_1(v) = \alpha_1 \sin\left((y_2(\varrho)) + \mu y_2(\varrho) \sin(y_3(\varrho))\right), \\ {}^{c}\Delta_b^{\beta} y_2(v) = \alpha_2 \sin(y_1(\varrho)) \sin(y_2(\varrho)), \\ {}^{c}\Delta_b^{\beta} y_3(v) = k y_2(\varrho), \end{cases} \tag{14}$$

where $\upsilon \in \mathbb{N}_{b+1-\beta}$, b is the initial point and $0 < \beta \leq 1$ represents the fractional order.

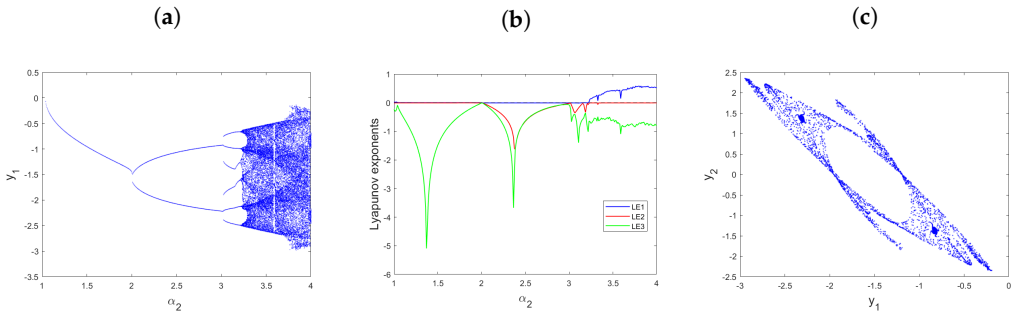

Figure 1. (**a**) Bifurcation diagram for α_2 ranging from 1 to 4. (**b**) The corresponding Lyapunov exponents. (**c**) Phase attractor of sine-based memristor map (12).

4. Nonlinear Dynamics of the Fractional-Order Sine-Based Memristor Map

In this section, we will conduct an analysis of the behaviors of the 3D fractional-order sine-based memristor map (14). The analysis will be carried out across commensurate and incommensurate orders. We will employ a range of numerical tools, such as visualizing phase portraits, illustrating bifurcations, and estimating the maximum Lyapunov exponent (LE_{max}).

4.1. Commensurate-Order Fractional Sine-Based Memristor Map

In this part, our focus is on elaborating on the different characteristics of the commensurate-order 3D fractional sine-based memristor map. It is important to recognize that a commensurate-order fractional system is comprised of equations that possess identical orders. To this end, we will now supply the numerical formula, which will be presented in the following manner and is derived from Theorem 1:

$$\begin{cases} y_1(r) = y_1(0) + \sum\limits_{j=0}^{r-1} \frac{\Gamma(r-j-1+\beta)}{\Gamma(\beta)\Gamma(r-j)} \Big(\alpha_1 \sin\big((y_2(j)) + \mu y_2(j) \sin\left(y_3(j)\right)\big)\Big), \\ y_2(r) = y_2(0) + \sum\limits_{j=0}^{r} \frac{\Gamma(r-j-1+\beta)}{\Gamma(\beta)\Gamma(r-j)} \Big(\alpha_2 \sin\left(y_1(j)\right) \sin\left(y_2(j)\right)\Big), \\ y_3(r) = y_3(0) + \sum\limits_{j=0}^{r} \frac{\Gamma(r-j-1+\beta)}{\Gamma(\beta)\Gamma(r-j)} \Big(k y_2(j)\Big). \end{cases} \tag{15}$$

Set $y_1(0) = -2$, $y_2(0) = 1$, and $y_3(0) = 0.1$ and the parameters to $\alpha_1 = 1.5$, $\alpha_2 = 3.8$, $\mu = 0.1$, and $k = 0.01$. Figure 2 displays the discrete-time evolution of the states y_1, y_2, and y_3 in the suggested commensurate 3D fractional sine-based memristor map (14) for $\beta = 0.25$. Additionally, Figure 3 illustrates the phase portraits for various values of the commensurate order β ($\beta = 0.05$, $\beta = 0.1$, $\beta = 0.3$, $\beta = 0.35$, $\beta = 0.9$, $\beta = 0.91$, $\beta = 0.95$, and $\beta = 1$). From the figures, it can be observed that the observed trajectories in the proposed commensurate map switch between hidden chaotic oscillations and periodic behaviors as the commensurate order β varies. Here, we plot three bifurcations of (14) associated with $\alpha_2 \in [0, 1]$, as shown in Figure 4, which correspond to the commensurate orders $\beta = 0.1$, $\beta = 0.3$, and $\beta = 0.95$. It is clear from the diagrams that there are distinct differences in the dynamics of the proposed map, underscoring the impact of both the system's parameters and the commensurate order on the states of the fractional sine-based memristor map (14). Certainly, it is evident that the dynamics of the system's states undergo a transition from periodic to chaotic behavior as the parameter α_2 increases, often accompanied by the emergence of periodic doubling bifurcation. For instance, when the commensurate order of β is set to 0.1, the map exhibits chaotic behavior within the range of α_2 between 1.9 and 4. Similarly, for $\beta = 0.3$, the chaotic region occurs for α_2 within the interval of $[3.8, 4]$. Furthermore, when $\beta = 0.9$, chaos is present when $\alpha_2 \in [3.3, 3.9]$. This delineation of chaotic regions across different parameter values provides valuable insights

into the intricate behavior of the commensurate-order fractional sine-based memristor map (14).

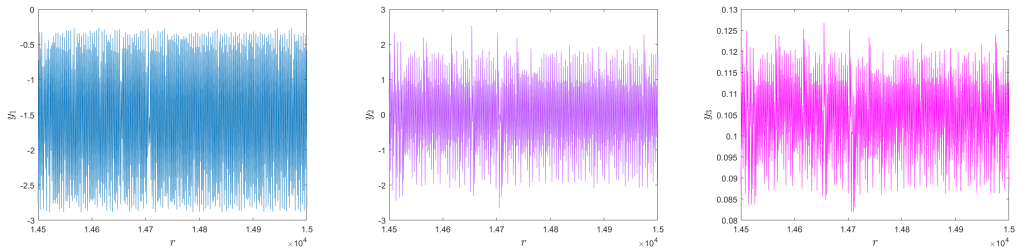

Figure 2. Time evolution of the commensurate 3D fractional sine-based memristor map (14) for $\beta = 0.25$.

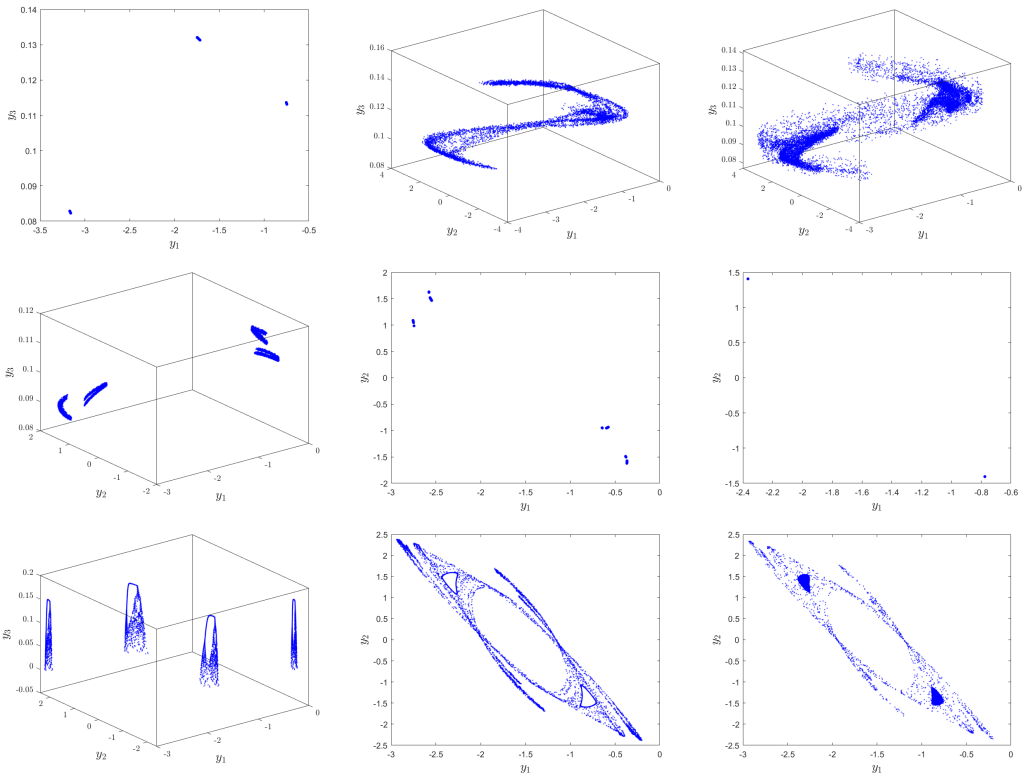

Figure 3. Phase portraits of (14) for different values of β: $\beta = 0.05, 0.1, 0.25, 0.3, 0.35, 0.9, 0.91, 0.95$ and 1.

In order to achieve a comprehensive understanding of the influence of the commensurate order, a bifurcation diagram is used to depict the variations in the behaviors of the commensurate sine-based memristor map (14) as the order β is varied from 0 to 1 with a step size of 0.001. Figure 5 depicts the bifurcation and the LE_{max}. We can see that upon changing the commensurate order, a rich set of dynamic characteristics, ranging from chaotic to regular, of the 3D fractional map are investigated with regard to the commensurate order β. Notably, when $\beta \in (0.02, 0.06)$, the bifurcation diagram unveils the presence of 7-period orbits, underscoring the periodic nature of the trajectories. In addition, when $\beta \in (0.35, 0.91)$, the trajectories exhibit regular patterns, characterized by 8-, 4-, and 2-period orbits. Furthermore, regions of chaos can be distinguished when β falls within the ranges $(0, 0.02)$, $(0.06, 0.35)$, and $(0.91, 1)$. During these ranges, the Lyapunov exponent (LE_{max}) also fluctuates between positive and negative values, indicating transitions between chaotic and non-chaotic behaviors in the system, providing additional evidence for the system's complex and diverse behavior and confirming the sensitivity of the sine-based memristor map to changes in the commensurate-order parameter β. Furthermore,

based on observing the maximum Lyapunov exponent, it can be concluded that when the maximum Lyapunov exponent is not positive, the commensurate sine-based memristor map exhibits regular oscillations. Conversely, the presence of chaotic oscillations is inferred when the exponent is positive. These results both emphasize the sensitivity of the system to changes in β and demonstrate the richness and complexity of the dynamical properties in the commensurate-order 3D fractional sine-based memristor map (14).

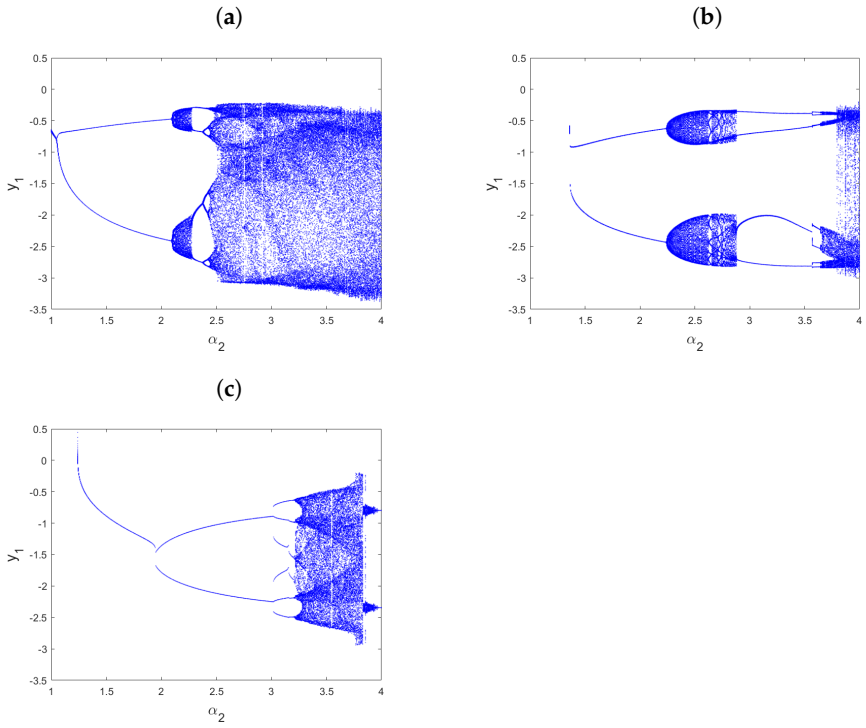

Figure 4. (**a**) Three Bifurcation diagrams of commensurate 3D fractional sine-based memristor map (14) with $\alpha_2 \in [1,4]$, for (**a**) $\beta = 0.1$, (**b**) $\beta = 0.3$, and (**c**) $\beta = 0.9$.

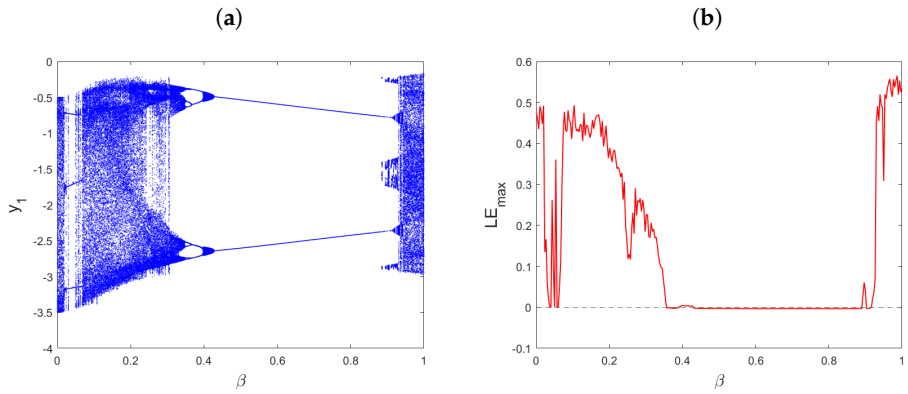

Figure 5. (**a**) Bifurcation of commensurate 3D fractional sine-based memristor map (14) for $\beta \in (0,1)$. (**b**) The corresponding LE_{max}.

4.2. Incommensurate-Order Fractional Sine-Based Memristor Map

In this section, we delve into the dynamics of the incommensurate-order 3D fractional sine-based memristor map. The concept of incommensurate order entails utilizing different fractional orders for each equation within the system. The representation of the incommensurate-order fractional sine-based memristor map is as follows:

$$\begin{cases} {}^{c}\Delta_{b}^{\beta_1} y_1(\upsilon) = \alpha_1 \sin\left((y_2(\varrho)) + \mu y_2(\varrho) \sin\left(y_3(\varrho)\right)\right), \\ {}^{c}\Delta_{b}^{\beta_2} y_2(\upsilon) = \alpha_2 \sin\left(y_1(\varrho)\right) \sin\left(y_2(\varrho)\right), \\ {}^{c}\Delta_{b}^{\beta_3} y_3(\upsilon) = k y_2(\varrho), \end{cases} \tag{16}$$

By utilizing Theorem 1, we can express the numerical representation of the incommensurate fractional 3D sine-based memristor map (16) as follows:

$$\begin{cases} y_1(r) = y_1(0) + \sum\limits_{j=0}^{r-1} \frac{\Gamma(r-j-1+\beta_1)}{\Gamma(\beta_1)\Gamma(r-j)} \left(\alpha_1 \sin\left((y_2(j)) + \mu y_2(j) \sin\left(y_3(j)\right)\right)\right), \\ y_2(r) = y_2(0) + \sum\limits_{j=0}^{r} \frac{\Gamma(r-j-1+\beta_2)}{\Gamma(\beta_2)\Gamma(r-j)} \left(\alpha_2 \sin\left(y_1(j)\right) \sin\left(y_2(j)\right)\right), \\ y_3(r) = y_3(0) + \sum\limits_{j=0}^{r} \frac{\Gamma(r-j-1+\beta_3)}{\Gamma(\beta_3)\Gamma(r-j)} \left(k y_2(j)\right), \end{cases} \tag{17}$$

We analyze the dynamics and characteristics of this map to understand its unique behavior and explore the implications of employing distinct fractional orders in the system's equations. Consider the same parameters and initial states shown previously. Figures 6 and 7 show the phase portraits and the time evolution of the states of the proposed incommensurate fractional 3D sine-based memristor map (16), respectively. One can observe that there is a difference between the phase portraits of the commensurate order and incommensurate order sine-based memristor maps, but it stays the same shape. Now, in Figure 8, an exploration of bifurcation behavior and their corresponding maximum Lyapunov exponent (LE_{max}) is conducted for the incommensurate-order 3D fractional sine-based memristor map (16). This investigation involves varying the orders β_1 (as depicted in Figure 8a), β_2 (as depicted in Figure 8b), and β_3 (as depicted in Figure 8c) from 0 to 1 with a step size of 0.001. From Figure 8a, it is evident that the state of the incommensurate sine-based memristor map (16) exhibits chaotic behavior across most values of β_1, as indicated by the presence of positive Lyapunov exponents, except for a relatively small region $[0.69, 0.71]$ in which the trajectories exhibit regular behavior. On the other hand, from Figure 8b, it can be observed that as the incommensurate order β_2 is altered, the trajectories undergo a transition state and oscillate between chaotic and periodic states. As β_2 drops and approaches 0, or when it increases close to 1, the states of the incommensurate fractional sine-based memristor map display chaotic attractors, where the LE_{max} displays their highest values. For the rest of the interval, especially when $\beta_2 \in [0.234, 0.505]$, the trajectories are totally regular. This dynamic underscores the sensitivity of the system to even minor changes in the incommensurate order β_2. Furthermore, the bifurcation chart and its corresponding largest Lyapunov exponent (LE_{max}), where the parameter β_3 is varied within the range $(0, 1)$, are presented in Figure 8c. Here, we maintain the incommensurate orders as $\beta_1 = \beta_2 = 1$. Figure 8c reveals a distinct behavior compared to the previous cases. The most prominent observation is the expansion of the chaotic region of the states of the incommensurate-order 3D fractional sine-based memristor map (16) across all values of β_3 within the interval of (0, 1), which is evident from the positive values of LE_{max}. The observed changes in the dynamic patterns of the proposed incommensurate fractional sine-based memristor map (16) illustrate the sensitivity to variations in the incommensurate orders β_1, β_2, and β_3, highlighting the complexity and versatility of the incommensurate-order 3D fractional sine-based memristor map.

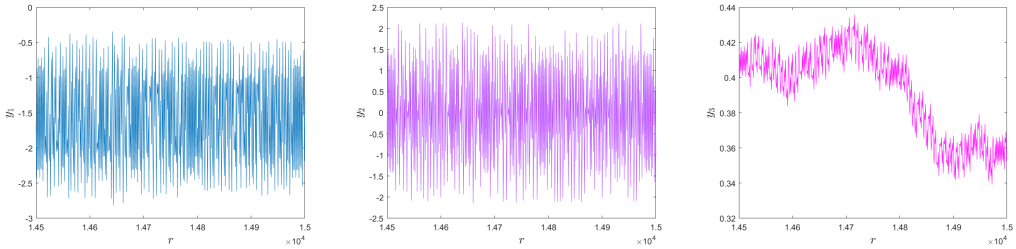

Figure 6. Time evolution of the incommensurate 3D fractional sine-based memristor map (16) for $\beta_1 = 0.9$, $\beta_2 = 1$, and $\beta_3 = 1$.

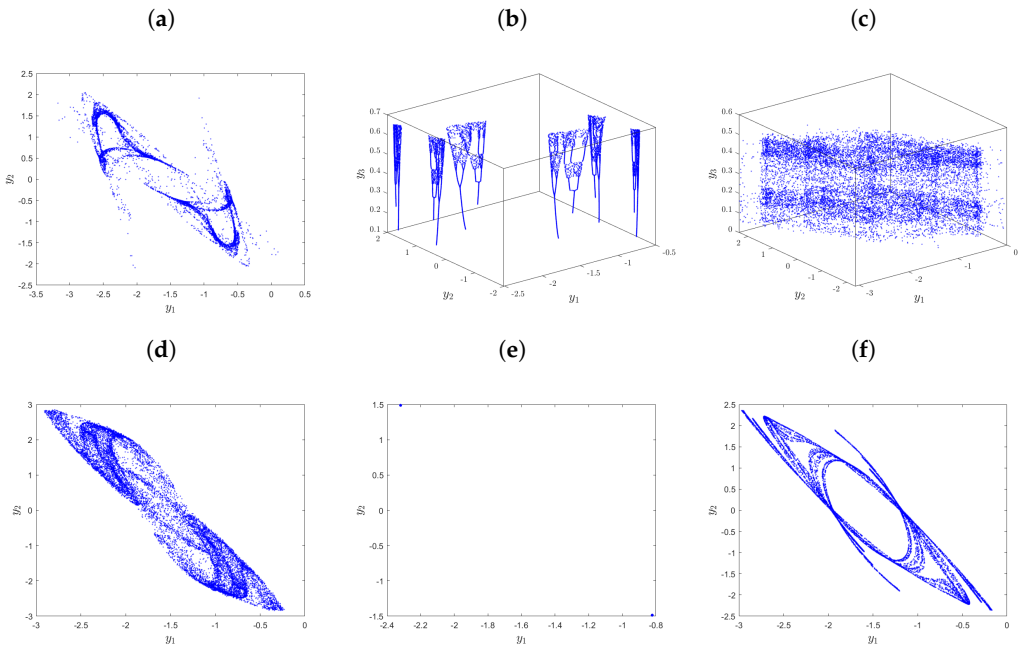

Figure 7. Phase portraits of (16) for different values of incommensurate orders β_1, β_2, and β_3 **(a)** $(\beta_1, \beta_2, \beta_3) = (0.6, 1, 1)$, **(b)** $(\beta_1, \beta_2, \beta_3) = (0.7, 1, 1)$, **(c)** $(\beta_1, \beta_2, \beta_3) = (0.9, 1, 1)$, **(d)** $(\beta_1, \beta_2, \beta_3) = (1, 0.6, 1)$, **(e)** $(\beta_1, \beta_2, \beta_3) = (1, 0.9, 1)$, **(f)** $(\beta_1, \beta_2, \beta_3) = (1, 1, 0.6)$.

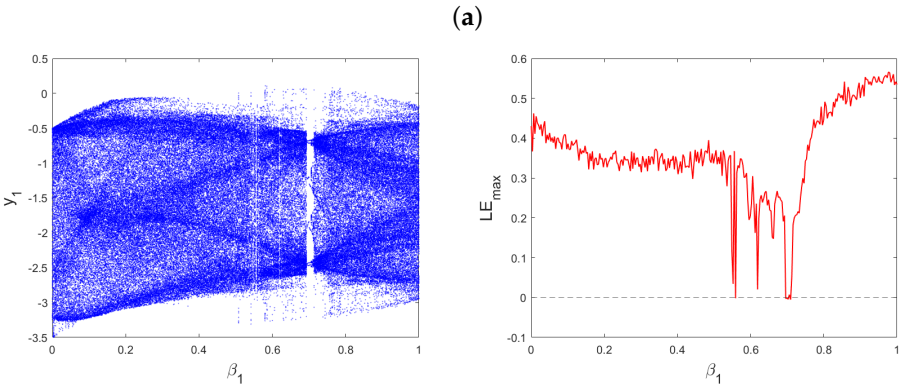

Figure 8. *Cont.*

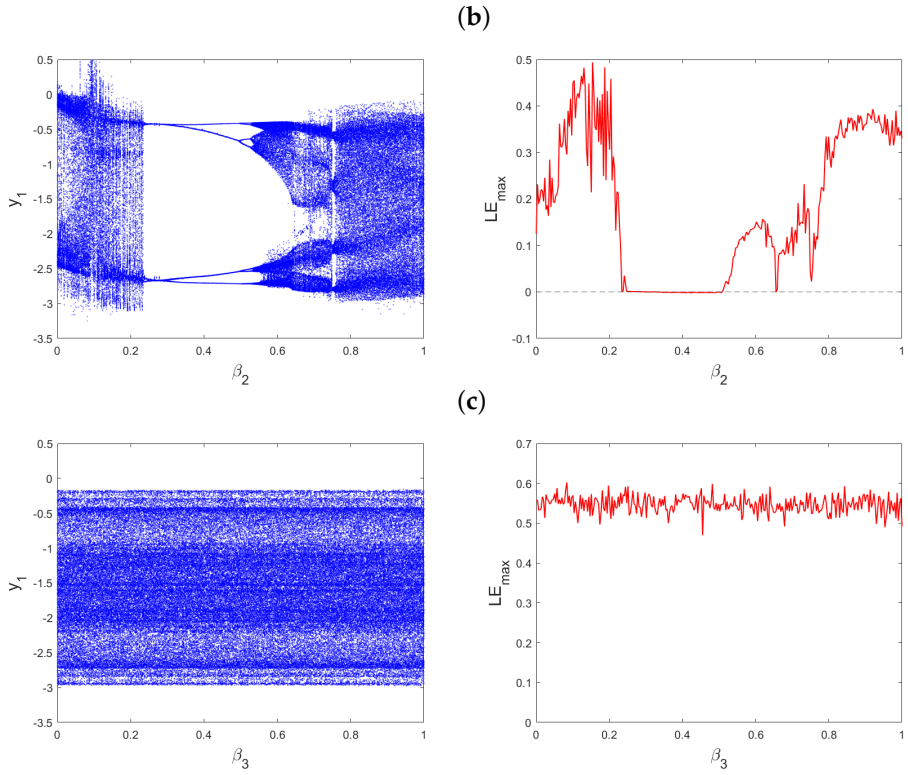

Figure 8. Bifurcation diagrams and their LE_{max} of incommensurate 3D fractional sine-based memristor map (16) for (**a**) $\beta_2 = \beta_2 = 1$, (**b**) $\beta_1 = 0.4$, $\beta_3 = 1$, and (**c**) $\beta_1 = \beta_2 = 1$.

To provide a more detailed illustration of the influence of incommensurate orders on the behaviors of the fractional sine-based memristor map (16), further investigation was carried out. These investigations offer a deeper understanding of how the fractional orders impact the system dynamics and underscore the importance of considering incommensurate orders in the analysis of the model's behavior. The three bifurcation diagrams presented in Figure 9 demonstrate the behaviors of the incommensurate fractional sine-based memristor map (16) as the parameter α_2 varies within the range [1, 4]. The simulations were conducted with parameter values of $\alpha_1 = 1.5$, $\rho = 0.1$, and $k = 0.01$ and the initial conditions $(y_1(0), y_2(0), y_3(0)) = (0 - 2, 1, 0.1)$. It is evident that these diagrams exhibit distinct patterns, indicating that the change in fractional orders $(\beta_1, \beta_2, \beta_3)$ significantly impacts the states of the incommensurate-order 3D fractional sine-based memristor map (16). For instance, when $(\beta_1, \beta_2, \beta_3) = (0.4, 1, 1)$, the system's states evolve from periodic to chaotic behavior with periodic doubling bifurcation as the parameter ρ increases. On the other hand, when $(\beta_1, \beta_2, \beta_3) = (1, 0.6, 1)$, oscillatory motion is observed, with trajectories remaining stable for small values of α_2 and becoming chaotic for large values of α_2, while, as $(\beta_1, \beta_2, \beta_3) = (0.4, 0.6, 1)$, chaos is present when $\alpha_2 \in [3.6, 4]$. These results emphasize the sensitivity of the incommensurate 3D fractional sine-based memristor map (16) to changes in the parameter α_2 and the incommensurate orders β_1, β_2, and β_3, resulting in a diverse range of nonlinear dynamic behaviors, including chaotic and periodic motion. This highlights the intricate and diverse nature of the incommensurate 3D fractional sine-based memristor map and the significance of the choice of incommensurate fractional orders in modeling and shaping its dynamics.

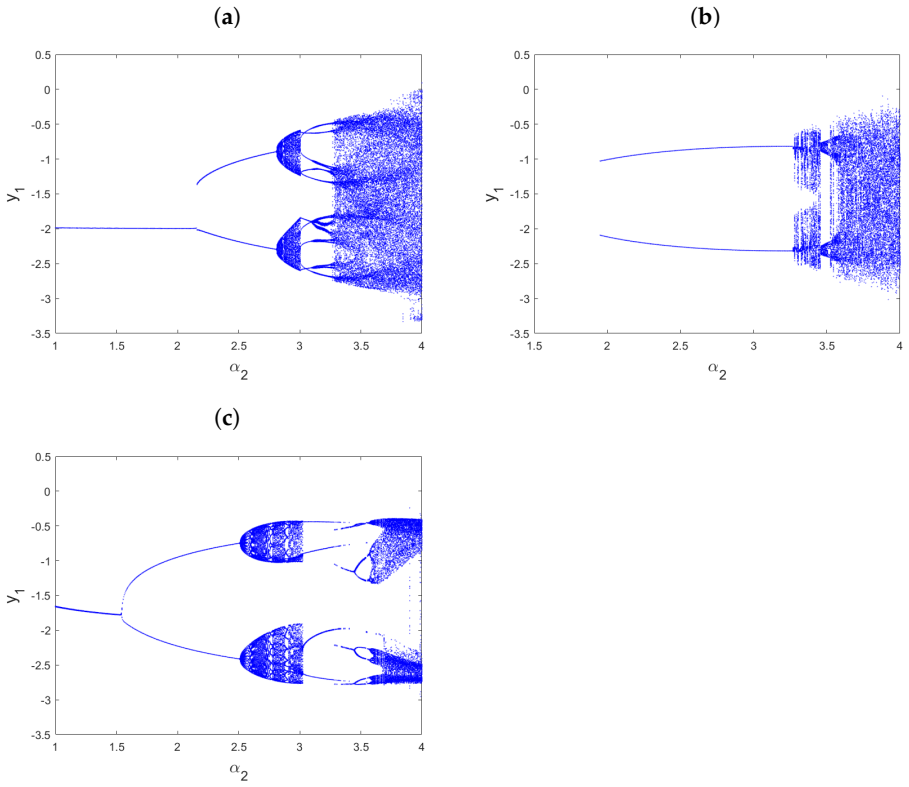

Figure 9. Bifurcations of (16) versus the parameter system α_2 for (**a**) $(\beta_1, \beta_2, \beta_3) = (0.4, 1, 1)$, (**b**) $(\beta_1, \beta_2, \beta_3) = (1, 0.6, 1)$, (**c**) $(\beta_1, \beta_2, \beta_3) = (0.4, 0.6, 1)$.

5. 0–1 Test and Complexity of Fractional Sine-Based Memristor Map

In the following, we examine the complexity of the proposed fractional sine-based memristor map with commensurate and incommensurate orders to assess its dynamical characteristics. A greater measure of complexity within a system is often indicative of a heightened degree of chaos. To this end, we employ both the sample entropy (*SampEn*) method and the C_0 complexity algorithm. Additionally, we utilize the 0–1 test to validate the presence of chaos within the fractional sine-based memristor map.

6. The Sample Entropy Test (*SampEn*)

In this study, we employ the sample entropy (*SampEn*) method to assess the complexity of both the commensurate-order fractional sine-based memristor map (14) and the incommensurate-order fractional sine-based memristor map (16). Unlike approximate entropy (*ApEn*), SampEn can effectively measure the irregularity of time series regardless of the embedding dimension (m) and the similarity coefficient (r). Consequently, *SampEn* provides a more consistent and unbiased measure compared to ApEn [39]. The SampEn values indicate the complexity level of the time series, with higher values corresponding to higher complexity [40]. The calculation of SampEn is performed as follows:

$$SampEn = -\log \frac{\Psi^{j+1}(r)}{\Psi^{j}(r)}, \tag{18}$$

where $\Psi^j(r)$ is expressed as

$$\Psi^{j}(r) = \frac{1}{m-j+1} \sum_{i=1}^{m-j+1} \log C_i^j(r). \tag{19}$$

and $r = 0.2std(C)$ is the tolerance defined and $std(C)$ represents the standard deviation.

The sample entropy results for the commensurate-order fractional sine-based memristor map (14) and the incommensurate-order fractional sine-based memristor map (16) are presented in Figure 10, with the initial conditions set as $(y_1(0), y_2(0), y_3(0)) = (-2, 1.0, 1)$ and the parameters set as $\alpha_1 = 1.5$, $\alpha_2 = 3.8$, $\mu = 0.1$, and $k = 0.01$. The obtained $SampEn$ values indicate the complexity levels of the time series, with larger values corresponding to higher complexity. The results demonstrate that both the commensurate and incommensurate fractional sine-based memristor maps exhibit higher complexity, as indicated by their larger $SampEn$ values. These findings align with the results obtained from the maximum Lyapunov exponent analysis, further confirming the chaotic nature of the dynamics in the proposed fractional system. The higher complexity and chaotic behavior support the significance of fractional orders in capturing the rich dynamics of the proposed fractional sine-based memristor map.

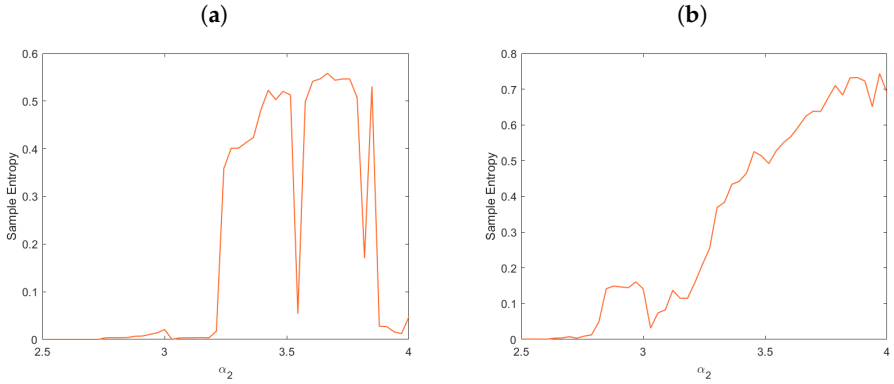

Figure 10. The sample entropy results of the fractional sine-based memristor map versus the parameter α_2 for (**a**) $\beta = 0.9$, (**b**) $(\beta_1, \beta_2, \beta_3) = (1, 0.6, 1)$.

6.1. The C_0 Complexity

To explore the influence of the fractional order on the dynamical characteristics of both the commensurate-order fractional sine-based memristor map (14) and the incommensurate-order fractional sine-based memristor map (16), the complexity analysis is measured using the C_0 complexity algorithm [41,42]. The inverse Fourier transform is used to calculate the C_0 complexity.

For a sequence $\{\sigma(0), \ldots, \sigma(D-1)\}$, we present the algorithm of the C_0 complexity as follows:

- The discrete Fourier transform of the sequence $\{\sigma(0), \ldots, \sigma(D-1)\}$ is determined:

$$\Theta_M(d) = \sum_{s=0}^{D-1} \sigma(s) \exp^{-2\pi i(sd/D)}, \qquad d = 0, \ldots, D-1. \tag{20}$$

- The mean square value is calculated as:

$$G_D = \frac{1}{D} \sum_{d=0}^{D-1} |\Theta_D(d)|^2. \tag{21}$$

- We set:

$$\bar{\Theta}_D(d) = \begin{cases} \Theta_D(d) & if \quad |\Theta_D(d)|^2 > rG_D, \\ 0 & if \quad |\Theta_D(d)|^2 \leq rG_D. \end{cases} \tag{22}$$

- The inverse Fourier transform of $\bar{\Theta}_D$ is given as follows:

$$\bar{\sigma}(d) = \frac{1}{D}\sum_{s=0}^{D-1} \bar{\Theta}(s)\exp^{2\pi i(ds/D)}, \quad d = 0,\ldots,D-1. \tag{23}$$

Finally, we evaluate the formula of the C_0 complexity by:

$$C_0 = \frac{\sum_{s=0}^{D-1} |\sigma(s) - \bar{\sigma}(s)|^2}{\sum_{s=0}^{D-1} |\sigma(s)|^2}. \tag{24}$$

Setting the initial condition $y_1(0) = -2$, $y_2(0) = 1$, and $y_3(0) = 0.1$ and the parameters to $\alpha_1 = 1.5$, $\alpha_2 = 3.8$, $\mu = 0.1$, and $k = 0.01$, the C_0 complexity of the commensurate-order fractional sine-based memristor map (14) and the incommensurate-order fractional sine-based memristor map (16) is described in Figure 11. These findings are consistent with the above results, indicating that the fractional sine-based memristor map has higher complexity. This indicates that the fractional-order sine-based memristor map with commensurate and incommensurate orders may generate chaotic attractors.

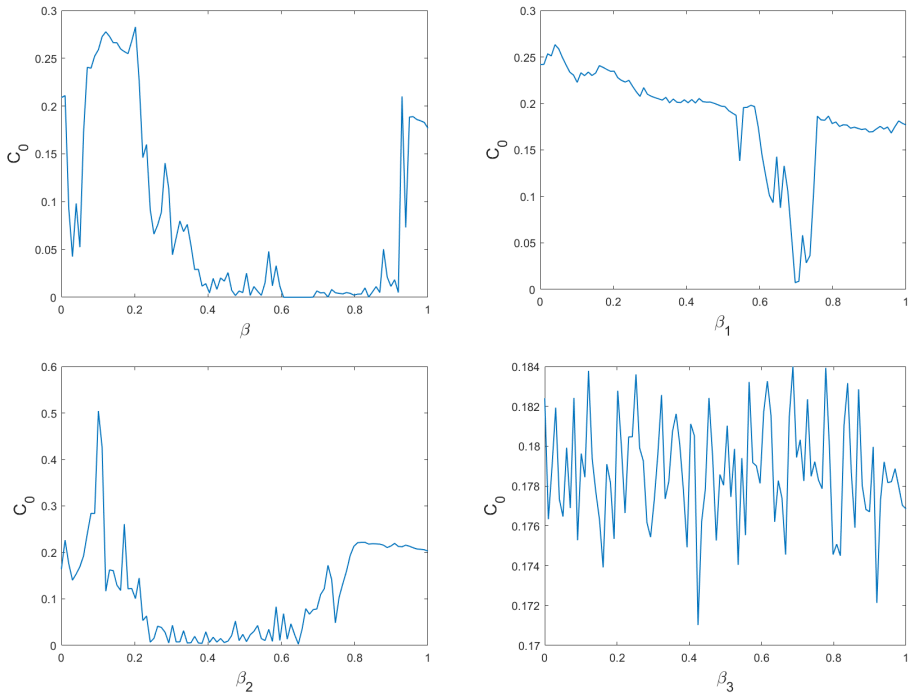

Figure 11. The C_0 complexity of the fractional sine-based memristor map versus commensurate and incommensurate orders.

The 0–1 Test for Chaos

Here, in order to establish the presence of chaos in both the commensurate-order fractional sine-based memristor map (14) and the incommensurate-order fractional sine-based memristor map (16), we utilize the 0–1 test method [43] for chaos. To represent this method, let $\{h(d), d = 1,2,\ldots..D\}$ be a set of states, and let the translation components p and q be given as:

$$p(d) = \sum_{\imath=1}^{d} h(\imath)cos(\imath c), \tag{25}$$

$$q(d) = \sum_{\imath=1}^{d} h(\imath)sin(\imath c), \tag{26}$$

where $d \in \{1, 2, \ldots . D\}$ and $c \in (0, \pi)$. The $(p - q)$ graph serves as a tool for discerning the presence or absence of chaos within the proposed fractional sine-based memristor map. By examining the trajectories of both p and q variables, important insights can be gained about the nature of the system's dynamics. When the trajectories of p and q remain bounded, it suggests that the map's dynamical behaviors are regular. Conversely, if these trajectories exhibit Brownian-like behaviors, it is indicative of chaotic dynamics within the map. Here, by employing p and q, the following formula is used to calculate the mean square displacement:

$$M_c = \frac{1}{D} \sum_{\iota=1}^{D} ((p(\iota + d) - p(\iota))^2 + (q(\iota + d) - q(\iota))^2), \qquad d < \frac{D}{10}. \tag{27}$$

We calculate the asymptotic growth rate as follows:

$$K_c = \lim_{d \to \infty} \frac{\log M_c}{\log d}. \tag{28}$$

and

$$K = median(K_c). \tag{29}$$

Thus, when K approaches 1, the system has a chaotic behavior, and when K approaches 0, the map is periodic. Figures 12 and 13 show the 0–1 test of the commensurate-order fractional sine-based memristor map (14) and the incommensurate-order fractional sine-based memristor map (16). Figures 12b and 13a clearly display bounded trajectories, proving that the system is periodic. Figures 12a,c and 13b,c corroborate the existence of chaotic movements on both the commensurate map and the incommensurate map by showing Brownian-like behaviors, which proves the presence of chaos. The findings of the 0–1 test are compatible with the maximum Lyapunov exponents (LE_{max}), sample entropy ($SampEn$) method, and C_0 complexity.

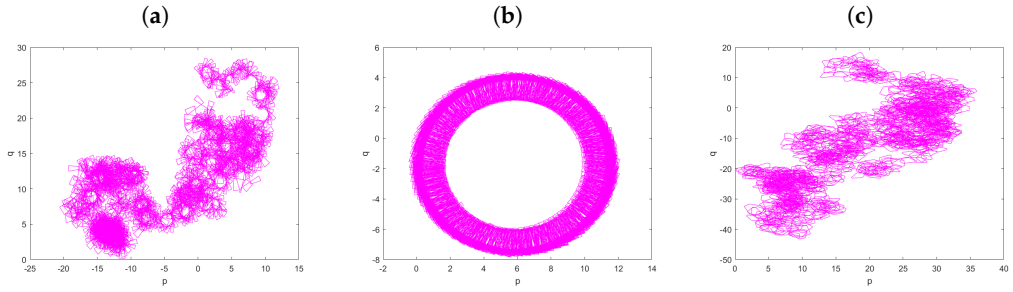

Figure 12. The $(p - q)$ plots of the commensurate fractional sine-based memristor map (14) for **(a)** $\beta = 0.25$, **(b)** $\beta = 0.91$, **(c)** $\beta = 0.95$.

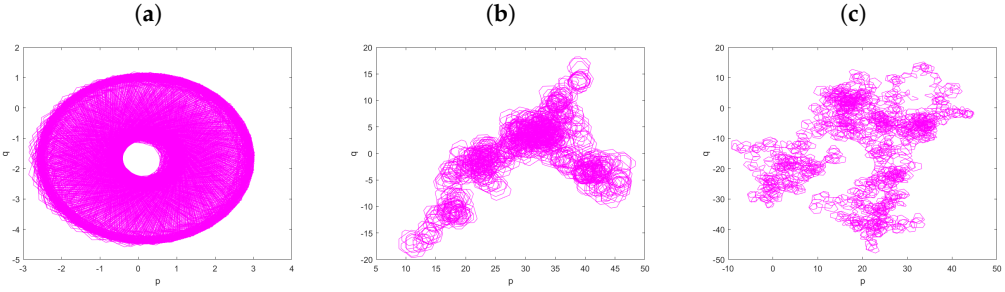

Figure 13. The $(p - q)$ plots of the incommensurate fractional sine-based memristor map (14) for **(a)** $(\beta_1, \beta_2, \beta_3) = (0.7, 1, 1)$, **(b)** $(\beta_1, \beta_2, \beta_3) = (1, 0.6, 1)$, **(c)** $(\beta_1, \beta_2, \beta_3) = (1, 1, 0.9)$.

7. Conclusions

By establishing a connection between the 2D sine map and the discrete memristor, the presented work introduced a novel 3D fractional-order sine-based memristor map based on the fractional Caputo-like difference operator. The dynamical properties of this map were thoroughly investigated under commensurate and incommensurate fractional orders. Through employing different methodologies of analysis involving Lyapunov exponent calculations, bifurcations, and phase portraits, the distinct behaviors of the proposed fractional sine-based memristor map were thoroughly explored across various scenarios. Furthermore, the complexity of the map was quantified using the sample entropy algorithm and C_0 complexity method, and the 0–1 test was used to validate the presence of chaos within the map. Through the numerical simulations conducted, the results underscored the strong influence exerted by the system parameters, the commensurate fractional order, and the incommensurate fractional orders on the states of the fractional sine-based memristor map, revealing numerous intriguing and diverse chaotic behaviors. The values of these parameters play a pivotal role in shaping the dynamics and behavior of the system, leading to variations in trajectories and responses in the state space of the suggested fractional sine-based memristor map. These findings hold significant value in elucidating the implications of fractional memristive maps, further enriching the field of chaotic dynamics and nonlinear systems.

Author Contributions: Conceptualization, T.H., A.A., G.M.G., W.M.M.S., M.S.A.S. and A.O.; Methodology, A.A., H.A.-T., G.M.G. and A.O.; Software, T.H., A.A., W.M.M.S. and M.S.A.S.; Validation, A.A. and A.O.; Formal analysis, A.A., H.A.-T., W.M.M.S., M.S.A.S. and A.O.; Investigation, T.H., A.A., H.A.-T., G.M.G., M.S.A.S. and A.O.; Resources, W.M.M.S.; Writing—original draft, A.A., H.A.-T., W.M.M.S. and A.O.; Writing—review & editing, T.H., A.A. and G.M.G.; Visualization, T.H., A.A., H.A.-T., G.M.G., W.M.M.S. and A.O.; Funding acquisition, T.H., H.A.-T., G.M.G. and M.S.A.S. All authors have read and agreed to the published version of the manuscript.

Funding: This research received no external funding.

Data Availability Statement: All data that support the findings of this study are included within the article.

Conflicts of Interest: The authors declare no conflict of interest.

References

1. Chua, L.O. Memristor-The missing circuit element. *IEEE Trans. Circuit. Theory* **1971**, *18*, 507–519. [CrossRef]
2. Strukov, D.B.; Snider, G.S.; Stewart, D.R.; Williams, R.S. The missing memristor found. *Nature* **2008**, *453*, 80–83. [CrossRef] [PubMed]
3. Ma, X.; Mou, J.; Liu, J.; Ma, C.; Yang, F.; Zhao, X. A novel simple chaotic circuit based on memristor—Memcapacitor. *Nonlinear Dyn.* **2020**, *100*, 2859–2876. [CrossRef]
4. Lin, T.C.; Huang, F.Y.; Du, Z.; Lin, Y.C. Synchronization of fuzzy modeling chaotic time delay memristor-based Chua's circuits with application to secure communication. *Int. J. Fuzzy Syst.* **2015**, *17*, 206–214. [CrossRef]
5. Sun, J.; Kang, K.; Sun, Y.; Hong, Q.; Wang, C. A multi-value 3D crossbar array nonvolatile memory based on pure memristors. *Eur. Phys. J. Spec. Top.* **2022**, *231*, 3119–3130. [CrossRef]
6. Bao, B.; Rong, K.; Li, H.; Li, K.; Hua, Z.; Zhang, X. Memristor-coupled logistic hyperchaotic map. *IEEE Trans. Circuits Syst. Regul. Pap.* **2021**, *68*, 2992–2996. [CrossRef]
7. Biswas, H.R.; Hasan, M.M.; Bala, S.K. Chaos theory and its applications in our real life. *Barishal Univ. J. Part.* **2018**, *1*, 123–140.
8. Pecora, L.M.; Carroll, T.L.; Johnson, G.A.; Mar, D.J.; Heagy, J.F. Fundamentals of synchronization in chaotic systems, concepts, and applications. *Chaos Interdiscip. J. Nonlinear Sci.* **1997**, *7*, 520–543. [CrossRef]
9. Lin, H.; Wang, C.; Du, S.; Yao, W.; Sun, Y. A family of memristive multibutterfly chaotic systems with multidirectional initial-based offset boosting. *Chaos Solitons Fractals* **2023**, 172, 113518. [CrossRef]
10. Lin, H.; Wang, C.; Yu, F.; Hong, Q.; Xu, C.; Sun, Y. A triple-memristor hopfield neural network with space multi-structure attractors and space initial-offset behaviors. *IEEE Trans.-Comput.-Aided Des. Integr. Circuits Syst.* **2023**, 1. [CrossRef]
11. Lin, H.; Wang, C.; Sun, Y. A universal variable extension method for designing multiscroll/wing chaotic systems. *IEEE Trans. Ind. Electron.* **2023**, 1–13. [CrossRef]
12. Yang, D.; Liu, Z.; Zhou, J. Chaos optimization algorithms based on chaotic maps with different probability distribution and search speed for global optimization. *Commun. Nonlinear Sci. Numer. Simul.* **2014**, *19*, 1229–1246. [CrossRef]

13. Chai, X.; Zheng, X.; Gan, Z.; Han, D.; Chen, Y. An image encryption algorithm based on chaotic system and compressive sensing. *Signal Process.* **2018**, *148*, 124–144. [CrossRef]
14. Xu, Q.; Sun, K.; Cao, C.; Zhu, C. A fast image encryption algorithm based on compressive sensing and hyperchaotic map. *Opt. Lasers Eng.* **2019**, *121*, 203–214. [CrossRef]
15. Ditto, W.; Munakata, T. Principles and applications of chaotic systems. *Commun. ACM* **1995**, *38*, 96–102. [CrossRef]
16. Vaidyanathan, S.; Volos, C. (Eds.) *Advances and Applications in Chaotic Systems*; Springer: Berlin, Germany, 2016; Volume 636, p. 445.
17. Zang, X.; Iqbal, S.; Zhu, Y.; Liu, X.; Zhao, J. Applications of chaotic dynamics in robotics. *Int. J. Adv. Robot. Syst.* **2016**, *13*, 60. [CrossRef]
18. Wang, X.; Su, Y.; Luo, C.; Nian, F.; Teng, L. Color image encryption algorithm based on hyperchaotic system and improved quantum revolving gate. *Multimed. Tools Appl.* **2022**, *81*, 13845–13865. [CrossRef]
19. Wu, G.C.; Baleanu, D. Discrete fractional logistic map and its chaos. *Nonlinear Dyn.* **2014**, *75*, 283–287. [CrossRef]
20. Abbes, A.; Ouannas, A.; Shawagfeh, N.; Khennaoui, A.A. Incommensurate fractional discrete neural network: Chaos and complexity. *Eur. Phys. J. Plus* **2022**, *137*, 235. [CrossRef]
21. Wang, M.; Wang, Y.; Chu, R. Dynamical analysis of the incommensurate fractional-order Hopfield neural network system and its digital circuit realization. *Fractal Fract.* **2023**, *7*, 474. [CrossRef]
22. Al-Qurashi, M.; Asif, Q.U.; Chu, Y.-M.; Rashid, S.; Elagan, S.K. Complexity analysis and discrete fractional difference implementation of the Hindmarsh–Rose Neuron System. *Results Phys.* **2023**, *51*, 106627. [CrossRef]
23. Abbes, A.; Ouannas, A.; Shawagfeh, N. An incommensurate fractional discrete macroeconomic system: Bifurcation, chaos, and complexity. *Chin. Phys. B* **2023**, *32*, 030203. [CrossRef]
24. Abbes, A.; Ouannas, A.; Shawagfeh, N.; Grassi, G. The effect of the Caputo fractional difference operator on a new discrete COVID-19 model. *Results Phys.* **2022**, *39*, 105797. [CrossRef] [PubMed]
25. Dababneh, A.; Djenina, N.; Ouannas, A.; Grassi, G.; Batiha, I.M.; Jebril, I.H. A new incommensurate fractional-order discrete 401 COVID-19 model with vaccinated individuals compartment. *Fractal Fract.* **2022**, *6*, 456. [CrossRef]
26. Saadeh, R.; Abbes, A.; Al-Husban, A.; Ouannas, A.; Grassi, G. The Fractional Discrete Predator–Prey Model: Chaos, Control and Synchronization. *Fractal Fract.* **2023**, *7*, 120. [CrossRef]
27. Li, C.; Feng, B.; Li, S.; Kurths, J.; Chen, G. Dynamic analysis of digital chaotic maps via state-mapping networks. *IEEE Trans. Circuits Syst. I Regul. Pap.* **2019**, *66*, 2322–2335. [CrossRef]
28. Peng, Y.; He, S.; Sun, K. Chaos in the discrete memristor-based system with fractional-order difference. *Results Phys.* **2021**, *24*, 104106. [CrossRef]
29. Lu, Y.M.; Wang, C.H.; Deng, Q.L.; Xu, C. The dynamics of a memristor-based Rulkov neuron with the fractional-order difference. *Chin. Phys. B* **2022**, *31*, 060502. [CrossRef]
30. Ma, M.; Lu, Y.; Li, Z.; Sun, Y.; Wang, C. Multistability and phase synchronization of Rulkov neurons coupled with a locally active discrete memristor. *Fractal Fract.* **2023**, *7*, 82. [CrossRef]
31. Shatnawi, M.T.; Abbes, A.; Ouannas, A.; Batiha, I.M. Hidden multistability of fractional discrete non-equilibrium point memristor based map. *Phys. Scr.* **2023**, *98*, 035213. [CrossRef]
32. Peng, Y.; Liu, J.; He, S.; Sun, K. Discrete fracmemristor-based chaotic map by Grunwald–Letnikov difference and its circuit implementation. *Chaos Solitons Fractals* **2023**, *171*, 113429. [CrossRef]
33. Khennaoui, A.A.; Pham, V.T.; Thoai, V.P.; Ouannas, A.; Grassi, G.; Momani, S. From Lozi map to fractional memristive Lozi map. *Eur. Phys. J. Spec. Top.* **2023**, 1–9. [CrossRef]
34. Atici, F.M.; Eloe, P. Discrete fractional calculus with the nabla operator. *Electron. J. Qual. Theory Differ. Equ.* **2009**, *2009*, 3. [CrossRef]
35. Abdeljawad, T. On Riemann and Caputo fractional differences. *Comput. Math. Appl.* **2011**, *62*, 1602–1611. [CrossRef]
36. Bao, H.; Hua, Z.; Wang, N.; Zhu, L.; Chen, M.; Bao, B. Initials-boosted coexisting chaos in a 2-D sine map and its hardware implementation. *IEEE Trans. Ind. Inform.* **2020**, *17*, 1132–1140. [CrossRef]
37. Bao, H.; Hua, Z.; Li, H.; Chen, M.; Bao, B. Discrete memristor hyperchaotic maps. *IEEE Trans. Circuits Syst. Regul. Pap.* **2021**, *68*, 4534–4544. [CrossRef]
38. Bao, B.C.; Li, H.; Wu, H.; Zhang, X.; Chen, M. Hyperchaos in a second-order discrete memristor-based map model. *Electron. Lett.* **2020**, *56*, 769–770. [CrossRef]
39. Richman, J.S.; Moorman, J.R. Physiological time-series analysis using approximate entropy and sample entropy. *Am. J. Physiol.-Heart Circ. Physiol.* **2000**, *278*, H2039–H2049. [CrossRef]
40. Li, Y.; Wang, X.; Liu, Z.; Liang, X.; Si, S. The entropy algorithm and its variants in the fault diagnosis of rotating machinery: A review. *IEEE Access* **2018**, *6*, 66723–66741. [CrossRef]
41. Shen, E.; Cai, Z.; Gu, F. Mathematical foundation of a new complexity measure. *Appl. Math. Mech.* **2005**, *26*, 1188–1196.
42. He, S.; Sun, K.; Wang, H. Complexity analysis and DSP implementation of the fractional-order Lorenz hyperchaotic system. *Entropy* **2015**, *17*, 8299–8311. [CrossRef]
43. Gottwald, G.A.; Melbourne, I. A new test for chaos in deterministic systems. *Proc. Math. Phys. Eng. Sci.* **2004**, *460*, 603–611. [CrossRef]